Case Studies in Thermal Engineering 75 (2025) 107003

Contents lists available at ScienceDirect

Case Studies in Thermal Engineering

journal homepage: www.elsevier.com/locate/csite

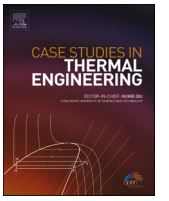

Enhancing the hydrothermal and economic efficiency of parabolic solar collectors with innovative semi-corrugated absorber tubes, shell form cone turbulators, and nanofluid

Sarminah Samad [a,*], Salman Saeidlou [b], M. Nadeem Khan [c], Ali Alamry [d], Laila M. Al-Harbi [e], Mohsen Sharifpur [f,g,h,**], S.P. Ghoushchi [i,***]

[a] Department of Management, College of Business Administration, Princess Nourah bint Abdulrahman University, Riyadh, 11671, Saudi Arabia
[b] School of Engineering, Technology and Design Canterbury Christ Church University Canterbury, Kent, UK
[c] Department of Mechanical and Industrial Engineering, Majmaah University, Al-Majmaah, 11952, Saudi Arabia
[d] Department of Mechanical Engineering, College of Engineering in Al-Kharj, Prince Sattam Bin Abdulaziz University, 11942, Al-Kharj, Saudi Arabia
[e] Chemistry Department, Faculty of Science, King Abdulaziz University, P.O. Box 80203, Jeddah, 21589, Saudi Arabia
[f] Department of Mechanical and Aeronautical Engineering, University of Pretoria, Private Bag X20, Hatfield, Pretoria, 0028, South Africa
[g] School of Mechanical, Industrial and Aeronautical Engineering, University of the Witwatersrand, Private Bag 3, Wits, 2050, South Africa
[h] Department of Medical Research, China Medical University Hospital, China Medical University, Taichung, Taiwan
[i] Sustainable Management of Natural Resources and Environment Research Group, Faculty of Environment and Labour Safety, Ton Duc Thang University, Ho Chi Minh City, Viet Nam

* Corresponding author.
** Corresponding author. Department of Mechanical and Aeronautical Engineering, University of Pretoria, Private Bag X20, Hatfield, Pretoria, 0028, South Africa.
*** Corresponding author.
E-mail addresses: sarminasamad@gmail.com (S. Samad), mohsen.sharifpur@up.ac.za (M. Sharifpur), sp.ghoushchi@yahoo.com (S.P. Ghoushchi).

https://doi.org/10.1016/j.csite.2025.107003

Available online 9 September 2025

G R A P H I C A L A B S T R A C T

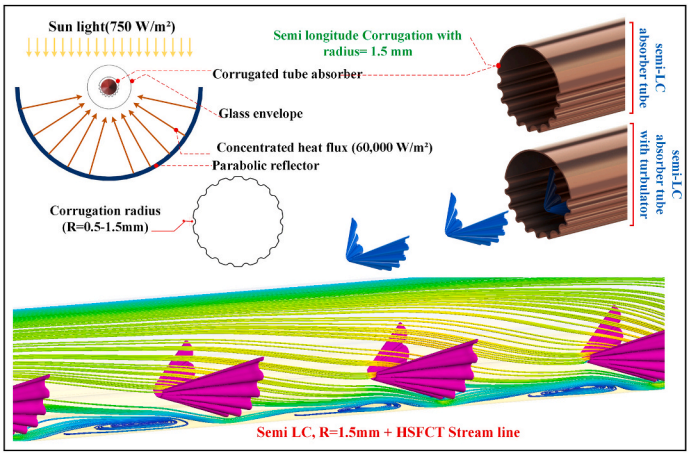

A R T I C L E I N F O

Keywords:
Parabolic trough solar collector
Semi-corrugated absorber tube
Shell form cone turbulators
Hydrothermal analysis
Economic analysis

A B S T R A C T

This study proposes a performance-enhancing design for parabolic trough solar collectors by integrating a novel semi-corrugated absorber tube with an innovative shell-form cone turbulator, operating with CuO–water nanofluid. Numerical simulations were conducted across a Reynolds number range of 4500–10,930 to evaluate the effects of corrugation radius (0.5–1.5 mm), nanofluid volume fraction (1–3 %), and turbulator geometry. Three turbulator designs—full (FSFCT), semi (SSFCT), and hollow (HSFCT) shell-form cone turbulators—were analyzed to identify optimal configurations. Performance was assessed from both hydrothermal and economic perspectives using the performance evaluation criterion (PEC), levelized cost of energy (LCOE), and payback time. Results indicate that the configuration combining a semi-corrugated tube with a 1.5 mm radius, 3 % CuO nanofluid, and the FSFCT achieved a 369 % increase in Nusselt number, an LCOE of 0.546 $/kWh, and a payback time of 3.6 years, confirming its economic superiority. From a thermal-hydraulic perspective, the highest PEC value of 2.77 was obtained using the HSFCT under the same conditions.

1. Introduction

The growing concerns about the finite nature of fossil fuels and their irreversible environmental impacts have intensified global interest in clean and sustainable energy alternatives. Among these, solar energy stands out due to its abundance, widespread availability, and potential to meet increasing global energy demands with a minimal ecological footprint. One of the most widely adopted technologies for harnessing solar energy is the parabolic trough solar collector (PTSC), which uses a curved reflector to concentrate sunlight onto a centrally positioned absorber tube. This focused solar radiation heats a working fluid flowing through the tube, enabling its use at elevated temperatures in various applications.

The critical importance of maximising solar energy utilization has prompted intensive research efforts aimed at improving the thermal efficiency of solar collectors through diverse innovative approaches. These strategies include augmenting the geometry of absorber tubes [1,2], integrating designs such as vortex generators and turbulator systems [1,3], using innovative nanofluids [4–6], and incorporating porous materials and phase change materials [7,8]. Such advancements can significantly improve the efficiency and performance of PTSCs, thereby reducing reliance on fossil fuels and offering substantial environmental benefits.

Existing studies have demonstrated that modifying absorber tube geometry can substantially enhance the thermal performance of solar collectors. For instance, Wang Fuqiang et al. [9] investigated the use of an outward corrugated absorber tube in a PTSC system to enhance thermal efficiency and reliability. Their findings showed a 148 % improvement in thermal performance compared to plain absorber tubes, though it resulted in a higher pressure drop. Akbarzadeh and Valipour [10] examined the impact of absorber tube corrugation on the hydrothermal performance of PTSCs under varying flow regimes and pitch ratios. Their findings confirmed that tube corrugation significantly enhances thermal performance, albeit with an associated increase in pressure drop. Mohammad Zaboli et al. [11] investigated the thermal performance of a PTSC enhanced with helical axial fins, which serve as swirl generators. The study

analyzed four absorber tube geometries and four inner helical fin pitches, ranging from 250 mm to 1000 mm. Results showed a notable thermal performance improvement of up to 23.1 % over plain tube configurations, highlighting the significant influence of fin pitch and fin geometry. Limboonruang et al. [12] studied the effect of employing an externally finned absorber tube in a PTSC. A numerical analysis was conducted on seven tube configurations with fin diameters ranging from 22 mm to 32 mm and pitch distances ranging from 3.63 mm to 2.28 mm. Results showed that the externally finned tube outperformed the smooth tube in thermal efficiency, with the best-finned tube achieving a temperature rise of 9.50 °C and thermal efficiency of 58.7 %, reflecting improvements of about 38 % and 41 % over smooth tubes. Moreover, the study revealed that smaller fin diameters provided greater thermal enhancement compared to larger ones.

In addition to absorber tube geometry, the incorporation of turbulators within the tube can significantly improve thermal performance. Moreover, their combined application often produces a synergistic thermal-economic performance enhancement. In a numerical study, Samad et al. [13]examined the effect of using spiral channeled conical turbulators on the thermal and economic performance of a PTSC. Various geometries of the turbulator were placed inside the absorber tube, and the results showed that this configuration could increase the Nusselt number by up to 375 % and enhance the collector's hydrothermal performance by a factor of 3.05. It was also found that the use of spiral channeled conical turbulators reduced the system's payback period and considerably decreased the operational costs associated with solar energy utilization. Bartosz Stanek et al. [14] studied how to improve heat absorption in PTSC by using a twisted tape turbulator with twisted ratios ranging from 1 to 4. The analysis demonstrated that including the twisted tape turbulator resulted in an extra 797.49 kWh of heat production during 1 year of operation. In a combined experimental and numerical investigation, Yasser Jebbar et al. [15] examined the impact of cylindrical turbulators on the hydrothermal performance of a PTSC. Their findings demonstrated that the incorporation of cylindrical turbulators within the absorber tube can enhance the thermal efficiency of the collector by up to 1.96 times compared to a conventional smooth-tube configuration. In a numerical study, Sultan Alshehery et al. [1] investigated the thermal performance enhancement of a PTSC by modifying the absorber tube geometry from circular to flat and incorporating a slashed triangular prism turbulator inside the tube. The results indicated that changing the tube geometry alone increased the Nusselt number by up to 46 %. Furthermore, the combined application of the flat absorber tube and the turbulator led to an even greater improvement, with the Nusselt number increasing by as much as 540 %. This study demonstrated that the simultaneous implementation of multiple heat transfer enhancement techniques can play a significant role in improving the thermal performance of solar collectors. Ramalingam Venkatesaperumal et al. [16], in an experimental study, investigated the effect of using a corrugated absorber tube instead of a traditional circular one on the thermal performance of a PTSC. To achieve additional enhancement, a conical strip turbulator was also installed inside the absorber tube, and its impact on hydrothermal characteristics was systematically analyzed. The results showed that both techniques individually improved the collector's thermal performance, while their combined application led to a synergistic enhancement in heat transfer.

Another effective approach to enhancing the performance of solar collectors and heat exchangers involves modifying the working fluid, such as employing nanofluids or incorporating phase change materials (PCMs). Moreover, combining these fluid-based techniques with other heat transfer enhancement methods, such as turbulators or improved tube geometries, can further amplify the overall thermal performance of system. M. Arun et al. [4] conducted a CFD-based investigation to evaluate the hydrothermal performance of PTSCs equipped with dimpled absorber tubes and operating with TiO_2–water nanofluids. Their results demonstrated that at a nanoparticle volume concentration of 0.3 % and a flow rate of 2.5 kg/min, the convective heat transfer coefficient improved by 34.25 %. These findings underscore the effectiveness of combining nanofluids with surface modifications in enhancing solar collector efficiency. Abdulelah Alhamayani and Moaz Al-lehaibi [6] studied energy and exergy efficiency enhancements in PTSC by adding Al_2O_3–TiO_2 hybrid nanoparticles to various fluids, including Syltherm-800, Solar Salt, and Therminol VP-1. Their simulations revealed that these nanoparticles simultaneously improved thermal performance and exergy efficiency across all tested fluids. Specifically, at inlet temperatures between 300 and 650 K, Therminol VP-1 with Al_2O_3–TiO_2 achieved a peak thermal efficiency of 71.68 %, while Syltherm-800 showed the highest exergy efficiency at 24.1 %. For operating temperatures above 500 K, Solar Salt-based nanofluid demonstrated superior average thermal and exergy efficiencies, reaching 61.8 % and 36.1 %, respectively.

In thermal–hydraulic studies of nanofluids, a central assumption is the Newtonian or non-Newtonian nature of the fluid, which depends on the nanofluid's type, properties, and the base fluid. Ayush Painuly et al. [17] conducted an experimental study on heat transfer and hydraulic performance in helically corrugated tubes fitted with triangular helical tape (THT) turbulators under laminar flow, employing water–ethylene glycol-based Al_2O_3–MWCNT hybrid nanofluids. Results showed that above 0.1 vol % particle loading, the fluid exhibited non-Newtonian behavior. Both higher nanoparticle concentration and lower helix ratio enhanced the Nusselt number and performance evaluation criterion (PEC). The maximum PEC of 2.31 occurred at $Re = 2000$ with 1 % hybrid nanofluid in a corrugated tube with a THT insert of helix ratio 2. Ayush Painuly et al. [18] conducted a numerical thermodynamic investigation of a non-Newtonian TiO_2–SiO_2 hybrid nanofluid, modeled within a water/ethylene glycol base, flowing through a corrugated tube under uniform wall heat flux. The analysis focused on the effects of corrugation height and nanoparticle volume fraction (1–5 %) on exergy destruction and entropy generation at flow rates between 15 and 25 L/min. The numerical findings demonstrated that both increased particle concentration and enhanced corrugation amplitude contributed to lowering entropy production and exergy losses. Furthermore, the combined application of the nanofluid and corrugated geometry yielded a substantial improvement in second-law performance, with exergetic efficiency reaching 82.8 % while overall irreversibilities were effectively suppressed. Ayush Painuly et al. [19] reported that SiC-MWCNT and Al_2O_3-MWCNT hybrid nanofluids exhibit Newtonian behavior below 0.1 % volume fraction in a water–ethylene glycol mixture, shifting to shear-thinning characteristics at higher concentrations, which affects their thermal–hydraulic performance in helically corrugated tubes. Praveen K. Namburu et al. [20] investigated the flow behavior of CuO nanoparticles dispersed in a 60:40 ethylene glycol–water blend. The study covered particle loadings between 0 % and 6.12 % and temperatures between −35 °C and 50 °C. Findings revealed that the nanofluids maintained Newtonian characteristics, with viscosity

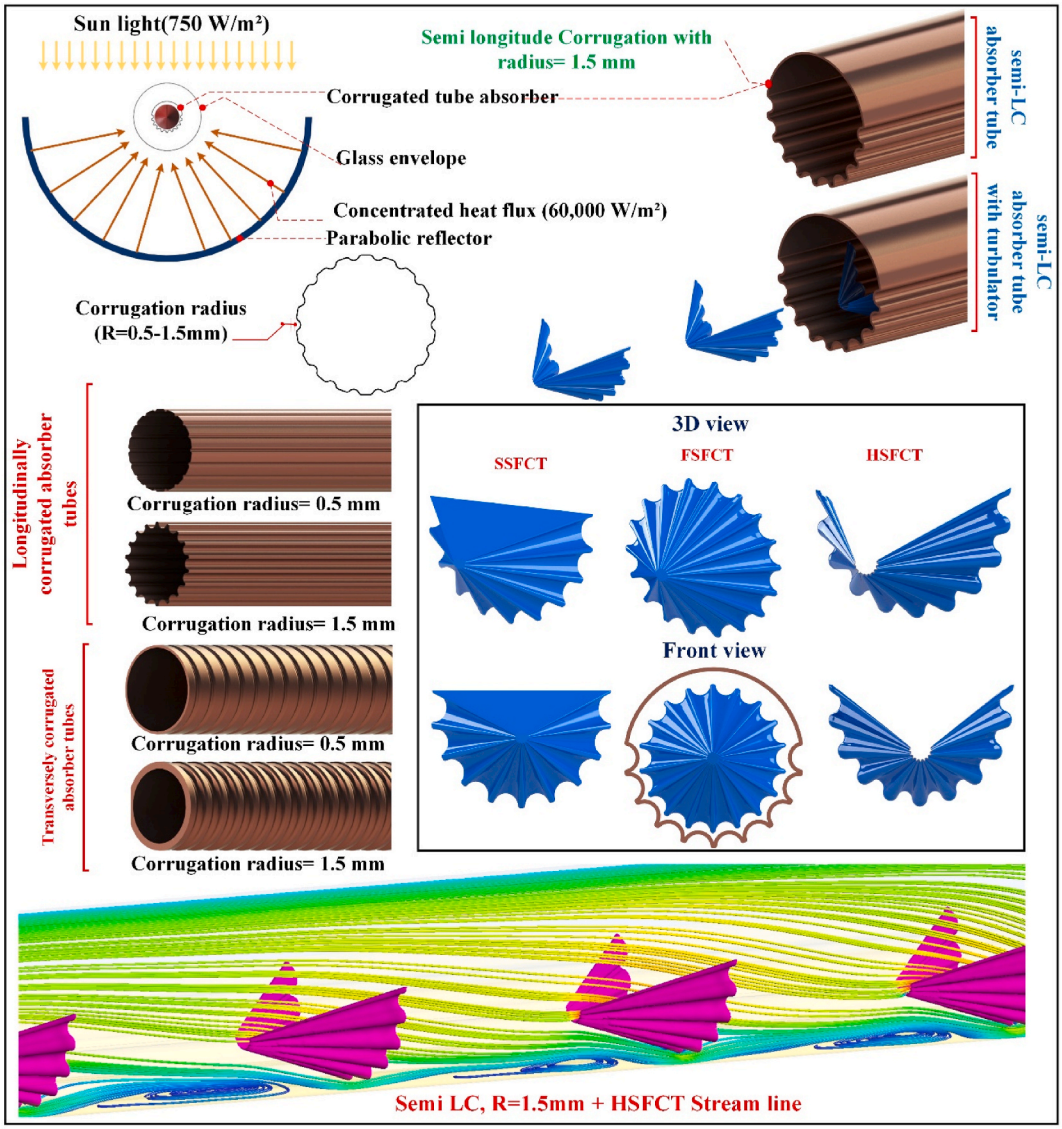

Fig. 1. Schematic view of the PTSC, corrugated tubes, and novel shell form cone turbulator (a), and sequence of the numerical study (b).

unaffected by shear rate. It should be noted that Mosavian et al. [21,22] reported CuO–water nanofluids behave as Newtonian up to a 3 % volume fraction, with non-Newtonian characteristics appearing at higher concentrations.

In light of the discussions presented, one promising approach to improve the performance of PTSCs is the selective surface corrugation of absorber tubes. Conventional corrugated absorber tubes are typically fully corrugated around their entire circumference. Since high heat flux occurs mainly on the lower half, corrugating the upper half yields minimal heat transfer enhancement but significantly increases pressure drop. To address this inefficiency, the present study proposes and investigates, for the first time, a novel semi-corrugated absorber tube design, where only the lower half of the inner surface is corrugated—strategically engineered to optimize heat transfer while minimizing unnecessary hydraulic losses. Another significant challenge in solar collectors is the development of boundary layers causing substantial temperature gradients in the working fluid. Specifically, the fluid temperature near the lower wall of the absorber tube—subject to high heat flux—can be significantly higher than at the tube center, leading to thermal inefficiencies. To mitigate this issue, the study introduces and evaluates an innovative shell form cone turbulator (SFCT), designed to disrupt the fluid flow, promoting uniform temperature distribution and enhancing turbulence and heat transfer across the tube's cross-section. This research evaluates the semi-corrugated absorber tube in three configurations: longitudinally corrugated (LC), transversely corrugated (TC), and the novel semi-longitudinally corrugated (semi-LC). Similarly, the SFCT turbulator is assessed in three distinct variants: full shell form cone turbulator (FSFCT), semi shell form cone turbulator (SSFCT), and hollow shell form cone

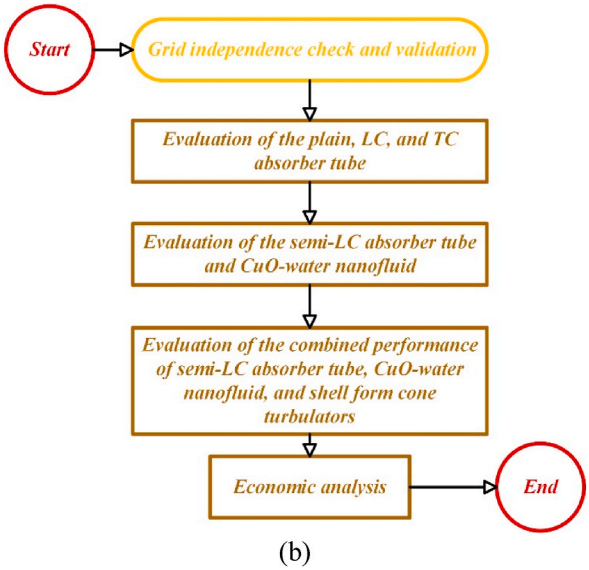

Fig. 1. (*continued*).

turbulator (HSFCT). Furthermore, to augment both thermal and economic performance, CuO-water nanofluids are employed as the working fluid. The combined application of these novel geometries and the use of nanofluids distinguishes this study from previous works, offering a comprehensive approach to enhance PTSC efficiency and cost-effectiveness under realistic operating conditions.

2. Methodology

2.1. Physical model definition

Fig. 1 illustrates a PTSC along with various geometries of the absorber tube and the shell form cone turbulator. The PTSC consists of two main components: a parabolic reflector that focuses solar energy onto the absorber tube and the absorber tube itself, which captures this energy to heat the working fluid. The absorber tube has a diameter of 22 mm and a length of 400 mm, and it is divided into two sections. The upper section, exposed to direct sunlight, receives a relatively low heat flux of approximately 750 W/m^2 [23,24]. In contrast, the lower section, subjected to concentrated energy from the parabolic reflector, experiences a significantly higher thermal flux of around 60,000 W/m^2 with a concentration ratio of 80 times. The study investigates four distinct designs of absorber tubes: a plain absorber tube, a longitudinally corrugated (LC) absorber tube, a transversely corrugated (TC) absorber tube, and a semi-longitudinally corrugated (semi-LC) absorber tube. Furthermore, the research examines the effect of corrugation radius (R), varying between 0.5 mm and 1.5 mm, on hydrothermal and economic performance. The analysis also includes the utilization of CuO-water nanofluids at different volume fractions (Φ) ranging from 1 % to 3 %, as well as the incorporation of a novel shell form cone turbulator featuring various geometries, including a full shell form cone turbulator (FSFCT), a semi-shell form cone turbulator (SSFCT), and a hollow shell form cone turbulator (HSFCT) within the absorber tube. This design is tailored for longitudinal corrugated tubes, allowing for precise alignment with the tube's corrugations. The study evaluates the influence of these factors on the friction coefficient, Nusselt number, performance evaluation criteria (PEC), and associated economic parameters.

In the initial phase of the numerical study, plain, LC, and TC absorber tubes were evaluated, each designed with a corrugation radius between 0.5 mm and 1.5 mm. The evaluation results were compared to identify the optimal geometry and corrugation radius, with the performance evaluation criteria (PEC) serving as the key metric. In the second phase of the study, following the identification of the optimal corrugated tube, a design modification was implemented to effectively manage the pressure drop and increase PEC. Specifically, only the lower section of the tube, which is subjected to high heat flux, was corrugated. This innovative design is introduced as the semi-longitudinally corrugated (semi-LC) absorber tube. CuO-water nanofluid was utilized as the working fluid, with volume fractions tested between 1 % and 3 %. Following a hydrothermal analysis of the semi-LC absorber tube and the CuO-water nanofluid, the PEC was calculated and compared against previous geometries to identify the most favorable option. In the subsequent phase of the study, a turbulator featuring an innovative geometry, comprising the FSFCT, the SSFCT, and the HSFCT, is introduced. The effects of these geometries on the heat transfer and friction coefficient of both the plain absorber tube and the semi-LC tube are evaluated, considering the presence and absence of CuO-water nanofluid. Ultimately, this analysis facilitates the identification of the most optimal hydrothermal configuration, as determined by the PEC. Finally, the last phase conducted an economic analysis of each geometry, determining the most economical option based on the levelized cost of energy (LCOE) and payback time metrics. The sequence of this numerical study is depicted in Fig. 1(b).

2.2. Mathematical formulations

This study outlines the governing equations for turbulent fluid flow, including continuity, momentum, and energy equations, as specified in Equations (1)–(3). The RNG k-ε model, detailed in Equations (4)–(6), also acts as supplementary equations for solving these three fundamental equations [25,26]. In formulating the governing equations, the fluid flow is considered incompressible and characterized as Newtonian, with its physical properties held constant. The analysis was performed assuming steady-state conditions, while the influence of gravity was deemed insignificant. Various auxiliary equations exist for addressing the RANS equations for turbulent flow, such as the standard k-epsilon and RNG k-epsilon, k-omega, among others. Research indicates that RNG k-epsilon yields a more precise solution compared to all other models for pipes fitted with turbulators [23,27,28].

Governing equations:

$$\frac{\partial(\rho u_i)}{\partial x_i}=0 \tag{1}$$

$$\rho\frac{\partial\left(u_i u_j\right)}{\partial x_j}=-\frac{\partial p}{\partial x_i}+\mu\frac{\partial}{\partial x_j}\left(\frac{\partial u_i}{\partial x_j}+\frac{\partial u_j}{\partial x_i}\right)+\rho\frac{\partial}{\partial x_j}\left(-\overline{u_j' u_i'}\right) \tag{2}$$

$$\frac{\partial}{\partial x_i}(\rho u_i T)=\frac{\partial}{\partial x_i}\left(\left(\frac{\mu_t}{Pr_t}+\frac{\mu}{Pr}\right)\frac{\partial T}{\partial x_i}\right) \tag{3}$$

Supplementary equations:

$$\frac{\partial}{\partial x_i}(\rho K u_i)=\frac{\partial}{\partial x_j}\left(\left(\frac{\mu_t}{\sigma_k}+\mu\right)\frac{\partial K}{\partial x_j}\right)+G_k-\rho\varepsilon \tag{4}$$

$$\frac{\partial}{\partial x_i}(\rho\varepsilon u_i)=\frac{\partial}{\partial x_j}\left(\frac{\partial\varepsilon}{\partial x_j}\left(\frac{\mu_t}{\sigma_k}+\mu\right)\right)+\frac{\varepsilon}{k}\left(C_{1\varepsilon}G_k-C_{2\varepsilon}\rho\frac{\varepsilon^2}{k}\right) \tag{5}$$

$$\left(\frac{\partial u_i}{\partial x_j}+\frac{\partial u_j}{\partial x_i}\right)\mu_t-\frac{2}{3}\mu_t\frac{\partial u_k}{\partial x_k}\delta_{ij}-\frac{2\delta_{ij}}{3}\rho K=\left(-\rho\overline{u_j' u_i'}\right) \tag{6}$$

In this context, the turbulent viscosity (μ_t) and the generation of turbulent kinetic energy (G_k) can be determined using specific equations (Equations (7) and (8)). Additionally, k represents the turbulent kinetic energy, while ε denotes the dissipation rate.

$$\mu_t=\rho\frac{1}{\varepsilon}C_\mu K^2 \tag{7}$$

$$G_k=-\rho u_j' u_i'\frac{\partial u_j}{\partial x_i} \tag{8}$$

2.3. Boundary conditions and numerical approach

In this research, the conditions at the tube inlet are set to a constant flow rate and a constant temperature. The upper wall is directly exposed to solar flux, while the heat flux at the bottom of the tube is assumed to be 80 times greater than the solar flux, owing to the concentration coefficient of the parabolic trough mirror. The tube outlet is treated as a pressure outlet, and the turbulator walls are adiabatic (indicating that the adiabatic characteristic of the turbulator wall does not contribute to heat transfer within the tube). The working fluid is incompressible and set in a steady state condition. The Simple C algorithm selected for linking the pressure and velocity fields aims to provide a quicker solution. Moreover, to achieve greater accuracy, a residual error threshold of e−5 has been applied to the equations of momentum, energy, and velocities, whereas the k and epsilon equations have been fine-tuned to e−6.

2.4. Hydrothermal characteristics calculation

To evaluate the thermal performance of parabolic trough solar collectors (PTSCs), the Nusselt number is commonly used as a key metric. This dimensionless number serves as a benchmark for assessing the effectiveness of various heat transfer enhancement techniques. The Nusselt number is calculated using Equation (9), which incorporates key parameters such as the absorber tube diameter (D) and the average heat transfer coefficient (h) [1,29–31].

$$Nu=\frac{hd_i}{k} \tag{9}$$

Also, h can be written as Equation (10) [1,29–31].

$$h=\frac{Q}{\pi d_i L\left(T_w-T_f\right)} \tag{10}$$

Where,

$$Q = \dot{m} c_p (T_o - T_i) \tag{11}$$

In this equation, T_i, T_o, T_w and T_f represent the working fluid inlet temperature, outlet temperature, mean temperature of the tube's inner surface, and mean temperature of the working fluid, respectively.

The friction coefficient and Reynolds number can be calculated using the formulas provided in Equations (12) and (13), as shown below [1]:

$$f = \frac{2D\Delta P}{(L\rho v^2)} \tag{12}$$

$$Re = \frac{\rho v D}{\mu} \tag{13}$$

Incorporating nanoparticles into the base fluid significantly alters its properties, including dynamic viscosity (μ), density (ρ), and heat capacity (k). The following equations are used to quantify these changes [32].

$$\rho_{nanofluid} = (1 - \Phi)\rho_{base\ fluid} + \Phi \rho_{nanoparticle} \tag{14}$$

$$\mu_{nanofluid} = \mu_{base\ fluid}(1 + 2.5\Phi) \tag{15}$$

$$\frac{k_{nanofluid}}{k_{base\ fluid}} = \frac{k_{nano\ particle} + 2k_{base\ fluid} + 2\Phi(k_{nano\ particle} - k_{base\ fluid})}{k_{nano\ particle} + 2k_{base\ fluid} - \Phi(k_{nano\ particle} - k_{base\ fluid})} \tag{16}$$

Simultaneously implementing corrugated tubes, nanofluids, and turbulators significantly impacts the Nusselt number and friction coefficient. A dimensionless factor that accounts for changes in both parameters is essential to evaluate and select the optimal hydrothermal configuration. The PEC is a widely adopted metric in studies focused on enhancing heat transfer. This parameter comprehensively assesses the trade-off between heat transfer augmentation and pressure drop. The PEC can be calculated using Equation (17) [1,33].

$$PEC = \frac{Nu}{Nu_0} \Big/ \left(\frac{f}{f_f}\right)^{1/3} \tag{17}$$

2.5. Economic analysis

A comprehensive evaluation of solar collectors must consider not only their hydrothermal performance but also their economic viability. Two key metrics are commonly used to assess the economic feasibility of solar collectors: the levelized cost of energy (LCOE) and the payback time [34]. The LCOE ($/kWh) provides a measure of the total cost ($) of generating a unit of solar energy (kWh) over the system's lifespan. In contrast, the payback time represents the time required to recoup this investment, measured in years. A lower LCOE and payback time indicate a more economically attractive option.

Economic evaluations of solar collector systems generally follow two main approaches. The first considers the total cost of all system components, including the PTSC, pumps, auxiliary equipment, and any additional expenses resulting from the implementation of thermal performance enhancement techniques such as turbulators and nanofluids. The second approach [26,34,35], which is adopted in the present study, focuses exclusively on the cost of the PTSC and the associated increase due to the use of enhancement methods. In this context, the LCOE is calculated using Equation (18). This equation takes into account the total amount of useful thermal energy generated (Q), which is obtained from Equation (11), and the total number of operating hours, assumed to be 24,000 h based on 1200 h per year over a 20-year operational lifespan. A key factor in this calculation is the collector cost (CO), which is estimated at $200/m^2 for a plain PTSC [34]. Any modification intended to enhance heat transfer—such as absorber tube corrugation, nanoparticle inclusion in the working fluid, or turbulator insertion—is assumed to independently increase CO. Specifically, the integration of a turbulator is estimated to raise the cost by approximately 3 % [26,35]. Based on fabrication cost estimates, absorber tube corrugation is assumed to contribute an additional 2 % to the total collector cost. Furthermore, the use of nanofluids with a 3 % volume fraction results in a 3 % increase in cost; this increase proportionally decreases with lower volume fractions.

$$LCOE = \frac{CO}{Q \times N} = \frac{CO}{\dot{m} c_p (T_i - T_o) \times N} \tag{18}$$

The payback time is calculated using Equation (19). This requires determining the cost of equivalent energy consumption (CE) under the same operating conditions, assuming electric heating as the baseline [35,36].

$$P_t = \frac{CO}{Q \times N \times CE} \tag{19}$$

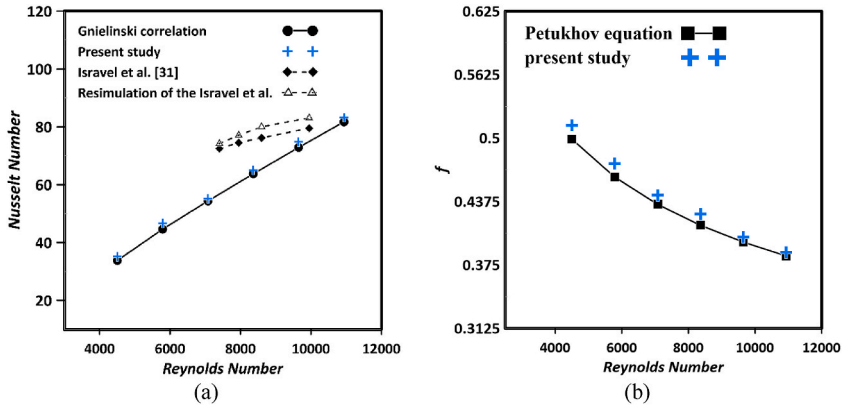

Fig. 2. (a) Validation of the *Nu* number using the Gnielinski equation and Isravel et al. study [37] (b): the friction coefficient using the Petukhov equation.

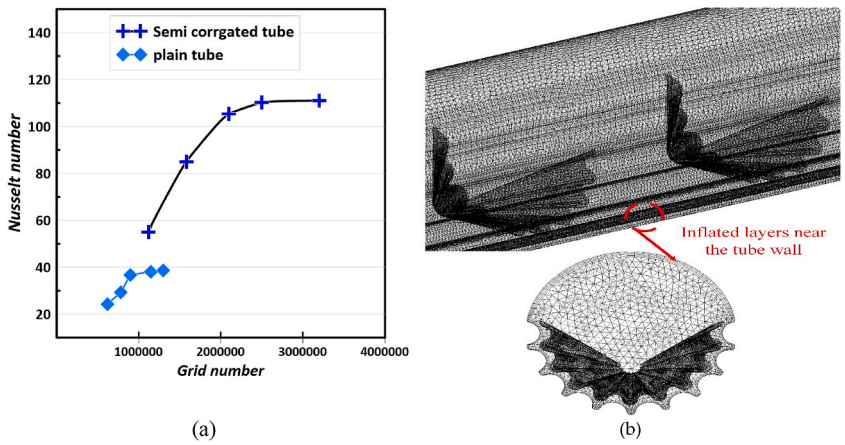

Fig. 3. (a): Grid independence check results (b): grid structure illustration.

3. Results

3.1. Grid independence check and validation

In numerical studies, two critical steps are necessary to ensure the accuracy and the mesh's integrity. The first step involves validating the numerical outcomes by comparing a plain absorber tube's friction coefficient and Nusselt number against established experimental correlations. The second step is conducting a grid independence check. For the validation process, the Nusselt number (*Nu*) of the plain absorber tube is assessed using the Gnielinski equation [1], while the friction coefficient is compared to the Petukhov equation [1]. To guarantee the accurate generation of the mesh and the proper application of boundary conditions, one scenario (a standard twisted tape with y/D = 20 mm) from the research conducted by Isravel et al. [37] has been precisely re-simulated, with the results displayed in Fig. 2 (a). The findings suggest that there is a reasonable deviation (maximum 7 %) between this study and the chosen scenario from Isravel et al. [37]. The results of this comparison are depicted in Fig. 2. The analysis indicates that the maximum discrepancies between the numerical results and their corresponding validated equations are 3.5 % for the Nusselt number and 2.9 % for the friction coefficient, suggesting a strong correlation between the numerical data and the validated equations. Furthermore, to verify consistent results across mesh counts, plain absorber tubes are tested with mesh counts ranging from 0.62 to 1.3 million, while semi-LC tubes are tested with mesh counts ranging from 1.12 to 3.2 million. Fig. 3 (a) demonstrates the correlation between the Nusselt number and mesh count. The results indicate that as the mesh count increases, reaching 0.9 million for the plain absorber tube and 2.5 million for the semi-LC absorber tube—the Nusselt number correspondingly rises. However, when the mesh count surpasses this, the changes in the Nusselt number become marginal, with the difference between consecutive Nusselt numbers dropping below 1.4 %. This finding highlights the independence of the results from mesh density at 0.9 million meshes for the plain absorber tube and 2.5 million meshes for the semi-LC absorber tube, establishing these mesh counts as the optimal selections for this study. Tetrahedral mesh is utilized to enhance mesh quality, with the average skewness and quality measured at 0.177 and 0.78, respectively (the closer the skewness approaches zero and the quality approaches one, the higher the overall quality of the mesh [38]. Moreover, Fig. 3 (b) shows

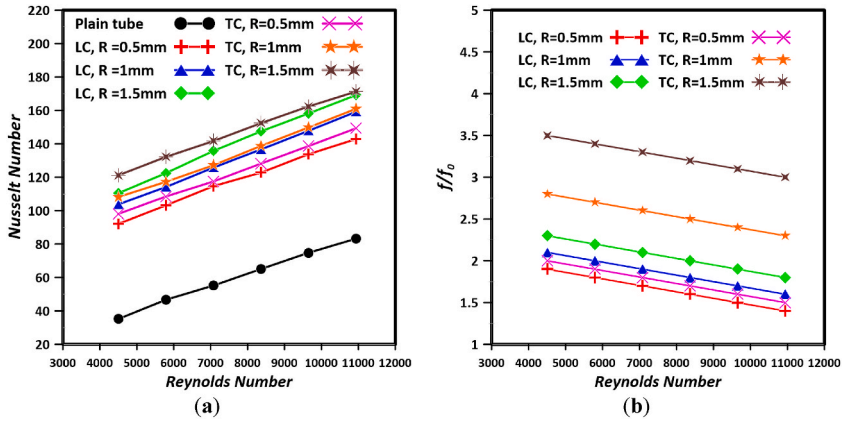

Fig. 4. Influence of longitudinal and transverse corrugation on the Nusselt number (a) and friction coefficient (b) across different corrugation radius.

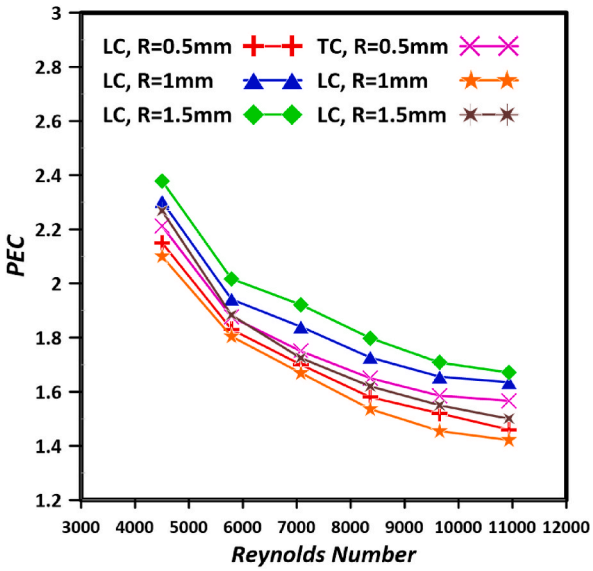

Fig. 5. Influence of longitudinal and transverse corrugation on the PEC across different corrugation radius.

the final mesh structure with inflated layers near the wall to capture the boundary layer behavior more accurately.

3.2. *Effect of the LC and TC absorber tube*

Two configurations of absorber tubes were examined to assess the impact of corrugated absorber tubes on the Nusselt number and friction coefficient: a longitudinally corrugated (LC) absorber tube and a transversely corrugated (TC) absorber tube. These results were compared to those obtained from a plain absorber tube. Numerical simulations were performed across a Reynolds number range of 4500 to 10,930, with the corrugation radius (R) changing from 0.5 mm to 1.5 mm. The Nusselt number and friction factor ratio are illustrated in Fig. 4(a) and (b).

The findings indicate that utilizing a corrugated absorber tube has a significant influence on the Nusselt number and the friction coefficient. Notably, the TC design demonstrated a more significant effect on heat transfer and friction coefficient than the LC design. Specifically, at a Reynolds number of 4500 and a corrugation radius of 0.5 mm, the Nusselt number for the TC absorber tube was up to 179 % higher. In contrast, the LC absorber tube exhibited a 162 % increase compared to the plain absorber tube. Another observation from Fig. 4 (a) is that increased corrugation radius leads to higher Nusselt number values. For instance, when utilizing a TC tube with a corrugation radius of 1.5 mm, the Nusselt number were found to be 23.5 %, than those measured with a 0.5 mm radius. Additionally, the results reveal a direct correlation between the Nusselt number and the Reynolds number, while the friction coefficient shows an inverse relationship with the Reynolds number. For example, at a Reynolds number of 10,900 and with a TC absorber tube having a corrugation radius of 1.5 mm, the Nusselt number was 41. 3 % higher compared to the values at a Reynolds number of 4500.

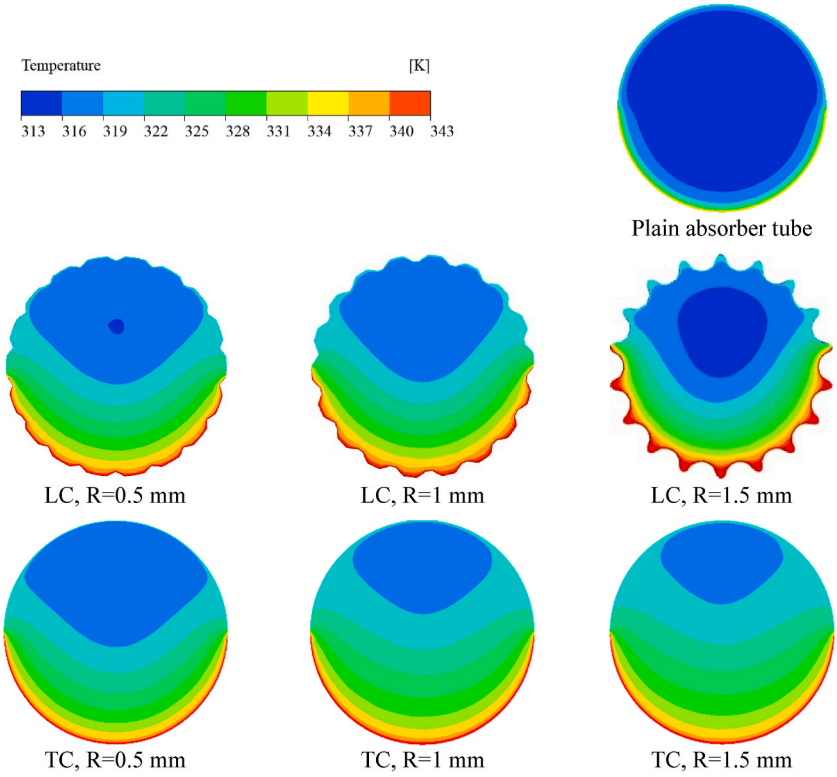

Fig. 6. Temperature contour for longitudinal and transverse corrugation across different corrugation radius.

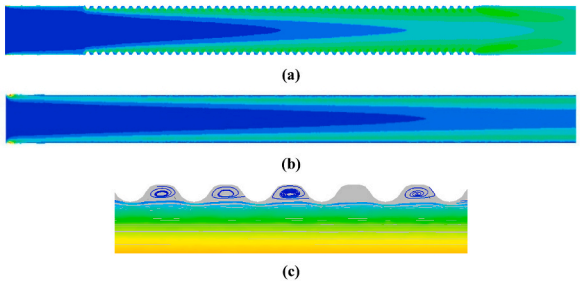

Fig. 7. Turbulence kinetic energy of the TC absorber tube with a corrugation radius of 1.5 mm (a), turbulence kinetic energy of the LC absorber tube with a corrugation radius of 1.5 mm (b), and swirling flows in the presence of corrugation (c).

Fig. 4 (b) illustrates the friction coefficient ratios for the two types of corrugations. It is evident that an increase in the radius of curvature for both TC and LC scenarios leads to a rise in pressure drop. For instance, in the LC scenario, the friction coefficient ratios for a radius of 0.5 mm and 1.5 mm are 90 % and 132 % greater than that of a plain pipe, respectively. In the TC scenario, these increases are 101 % and 253 % higher than those of a plain pipe. In general, there are two key points to consider regarding the increase in pressure drop. Firstly, as the radius of the corrugations expands, the contact surface area also enlarges, leading to an increase in frictional pressure drop. In the case of TC, this rise in pressure drop is attributed to both the heightened frictional pressure drop and the vortex-induced pressure drop resulting from the unique shape of the TC. A close examination of the streamlines depicted in Fig. 7 (c) reveals that the fluid flow with TC encounters a vortex near the walls, which contributes to greater fluid energy dissipation. Ultimately, these vortices result in a significantly larger increase in pressure compared to the LC case.

The impact of surface corrugation on the Nusselt number and friction coefficient is mainly due to the increased effective surface area of the tube. Corrugations increase the heat exchange surface, resulting in improved heat transfer rates and a higher average outlet temperature of the working fluid, as shown in Fig. 6. A larger corrugation radius corresponds to a greater heat exchange surface area, further enhancing heat transfer and average outlet temperature. TC absorber tubes outperform LC ones, as the former's design causes continuous fluctuations in effective cross-sectional area (or hydraulic diameter). This variation inhibits the thermal boundary layer's development, fostering swirling flows near the tube wall, which enhances heat transfer, as illustrated in Fig. 7 (c). As can be seen in

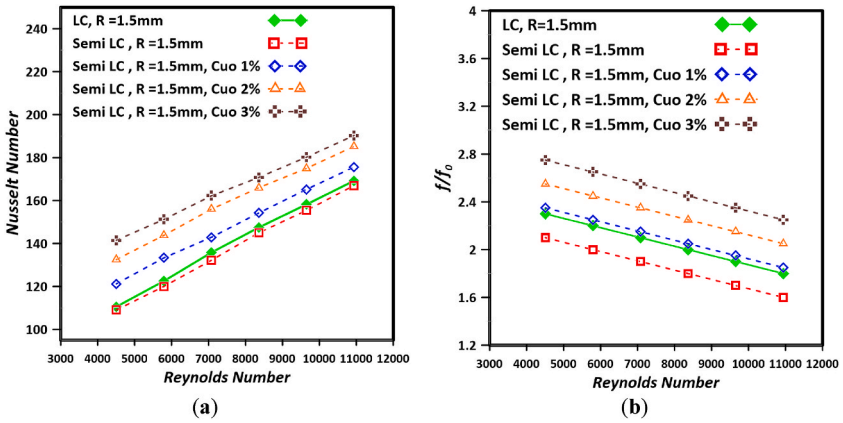

Fig. 8. Influence of semi-LC absorber tube and CuO-water nanofluid on the Nusselt number (a) and friction coefficient (b).

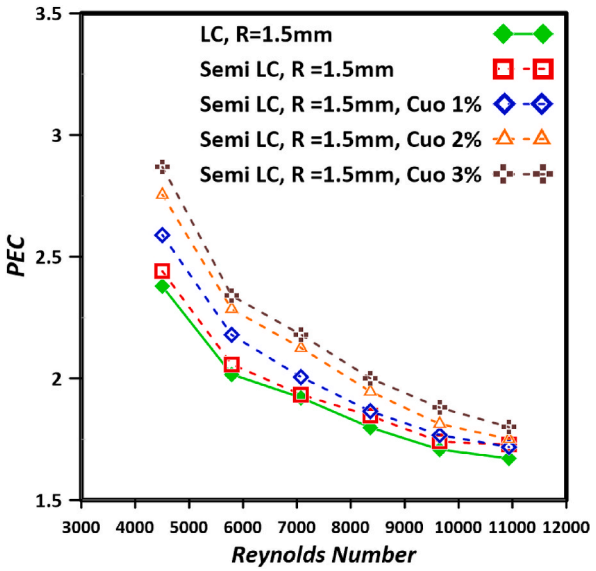

Fig. 9. Influence of semi-LC absorber tube and CuO-water nanofluid on the PEC.

Fig. 7(a) and (b), the increased turbulence kinetic energy in TC tubes also contributes to their superior performance.

The PEC has been utilized to identify the absorber tube's optimal geometry and corrugation radius. PEC is a dimensionless parameter influenced by both the Nusselt number and the friction coefficient, making it an effective tool for optimizing geometries based on hydrothermal performance. Fig. 5 illustrates the comparison of PEC across different geometries within a Reynolds number range of 4500 to 10,930. Even though the Nusselt number for the LC tube is lower than that of the TC tube, the PEC for the LC tube is superior due to its reduced friction coefficient. Remarkably, the peak PEC for the LC tube is 2.38, which is achieved with a corrugation radius of 1.5 mm. In contrast, the TC tube shows different behaviors at varying Reynolds numbers: at low Reynolds numbers, the highest PEC is also observed at a corrugation radius of 1.5 mm, while at high Reynolds numbers, the peak PEC occurs with a corrugation radius of 0.5 mm.

3.3. Effect of semi-LC absorber tube and nanofluid

LC absorber tubes with a corrugation radius of 1.5 mm were identified as the optimal hydrothermal solution. To further enhance performance, a novel geometry known as semi-LC absorber tubes was introduced. This design effectively increases PEC while simultaneously managing the friction coefficient. The semi-LC absorber tube retains a geometry similar to that of LC absorber tubes but only corrugates the lower section of the tube, which experiences high heat flux. This targeted corrugation enhances the heat transfer surface area and generates turbulence specifically in the area of most significant importance, thereby preventing excessive increases in the friction coefficient. Additionally, this study aimed to improve the thermodynamic characteristics of the working fluid by incorporating CuO nanoparticles. To enhance heat transfer and PEC, CuO nanoparticles were added to the base fluid (water) at three

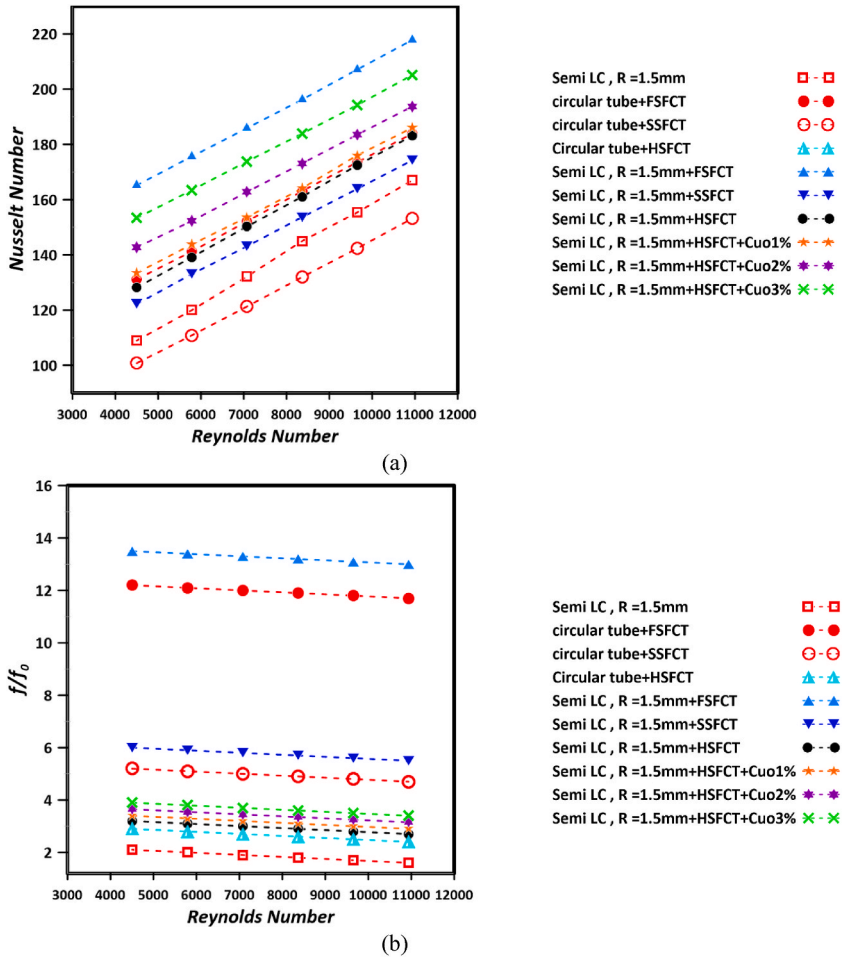

Fig. 10. Influence of the simultaneous usage of semi-LC absorber tube, CuO-water nanofluid, and shell form cone turbulator on the Nusselt number (a) and friction coefficient (b).

different volume fractions ranging from 1 % to 3 %. Fig. 8 (a), (b), and Fig. 9 illustrate the variations in Nusselt number, friction coefficient, and PEC concerning the Reynolds number for the semi-LC absorber tube, respectively, both with and without CuO nanoparticles. The results show that the Nusselt number for the semi-LC absorber tube, featuring a corrugation radius of 1.5 mm and functioning at a Reynolds number of 4,500, is 212.5 %. In comparison, the full corrugated tube exhibits an enhancement of 214.7 % relative to a plain tube. This indicates a difference of just 2.2 % lower than that of the LC absorber tubes. Since the upper part of the tube experiences minimal heat flux, the lack of corrugation in this region has a limited impact on heat transfer. The incorporation of CuO nanoparticles into the base fluid significantly enhances thermal conductivity and thermodynamic properties, leading to an increase in the Nusselt number. The findings show that at a Reynolds number of 4,500, the addition of CuO nanoparticles at volume fractions of 1 %, 2 %, and 3 % resulted in increases in the Nusselt number of 244.3 %, 276.4 %, and 302 %, respectively.

Upon reviewing Fig. 8 (b), it is clear that the fully corrugated tube increases the friction coefficient by 132 % in comparison to a plain tube at a Reynolds number of 4500, whereas the semi-corrugated tube shows an increase of 113 %. The noted decreases in the friction coefficient can be linked to the lack of corrugation in the upper part of the tube, which inherently results in lower friction coefficients. However, it is essential to note that nanoparticles possess a higher viscosity than the base fluid, and their addition raises the fluid's viscosity overall. This increased viscosity results in more considerable resistance to flow, which, in turn, elevates the friction coefficient. As illustrated in Fig. 8 (b), incorporating 1 %, 2 %, and 3 % nanofluid into the base fluid in the presence of a semi-LC tube enhances the friction coefficient by 135 %, 156.5 %, and 175.7 % respectively, when compared to the plain tube. This rise indicates that incorporating 3 % nanofluid into the base fluid in the presence of a semi-LC tube can enhance the friction coefficient by as much as 62.7 % in comparison to water fluid.

Fig. 9 depicts the PEC for all the scenarios outlined. From this figure, it is apparent that the initial change in PEC increases with the semi-LC tube, and at the first tested Reynolds number, the PEC for a corrugation radius of 1.5 mm is 2.44, while for a full LC tube under identical conditions, the PEC is 2.38. This improvement is certainly due to the reduction in pressure drop caused by the elimination of the upper corrugation of the tube. The maximum PEC of 2.67 occurs when CuO nanoparticles are used at a volume fraction of 3 %

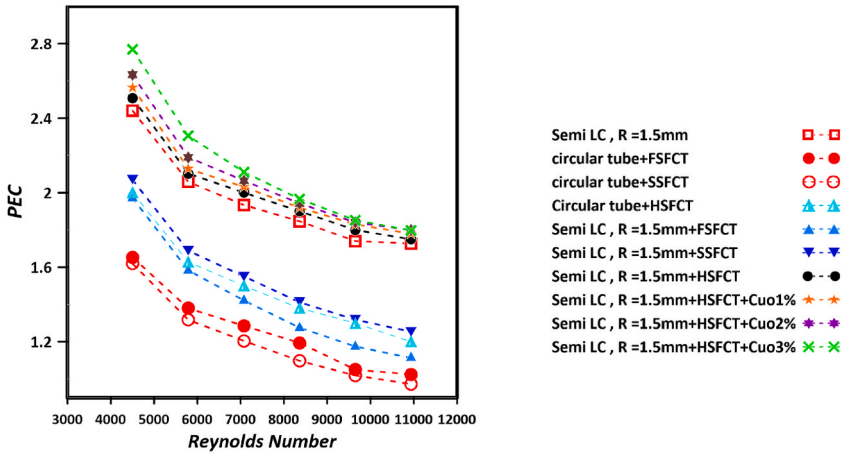

Fig. 11. Influence of the simultaneous usage of semi-LC absorber tube, CuO-water nanofluid, and shell form cone turbulator on the PEC.

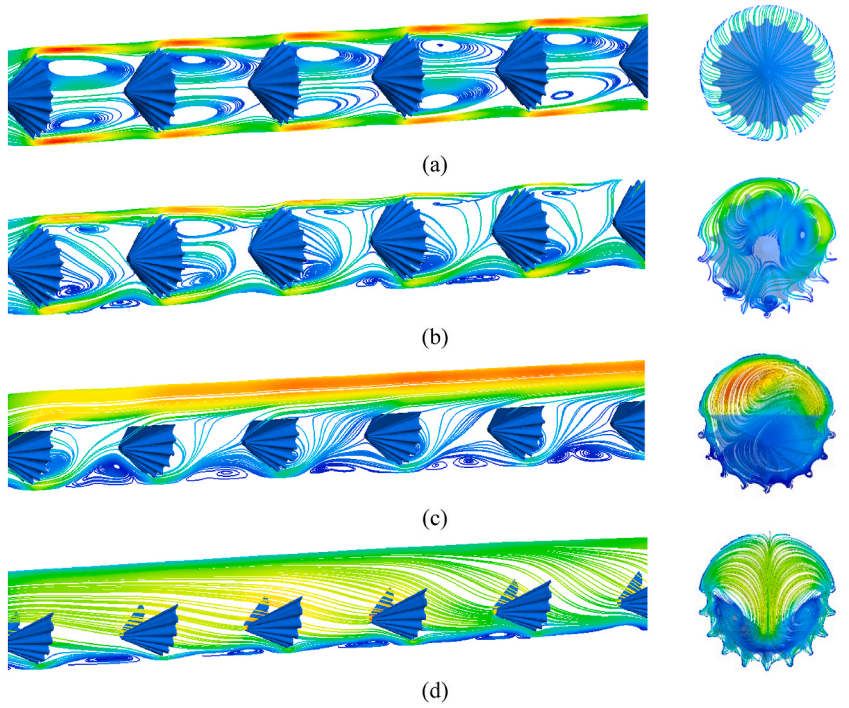

Fig. 12. Streamline in the plain tube equipped with FSFCT (a) and streamline in the Semi-LC tube equipped with FSFCT (b), SSFCT (c), and the HSFCT (d).

within a semi-LC absorber tube at a Reynolds number of 4500. Notably, this PEC value is 17.5 % higher than that of the semi-LC absorber tube without CuO nanoparticles.

3.4. Effect of simultaneous usage of three passive methods

In this segment of the study, an innovative shell form cone turbulator featuring various configurations is introduced and analyzed: the full shell form cone turbulator (FSFCT), the semi-shell form cone turbulator (SSFCT), and the hollow shell form cone turbulator (HSFCT). The investigation encompasses not only the independent effects of these turbulators on the heat transfer characteristics and friction coefficients of a plain tube heat exchanger but also their simultaneous application with an optimized corrugated tube (1.5 mm radius semi-LC absorber tube) and CuO-water nanofluid across various volume fractions. The objective is to maximize the Nusselt number and the PEC. Figs. 10 and 11 display the variations of the Nusselt number, friction coefficient, and PEC as functions of the Reynolds number for each method—both separately and together. The results reveal that employing the FSFCT, SSFCT, and HSFCT in a

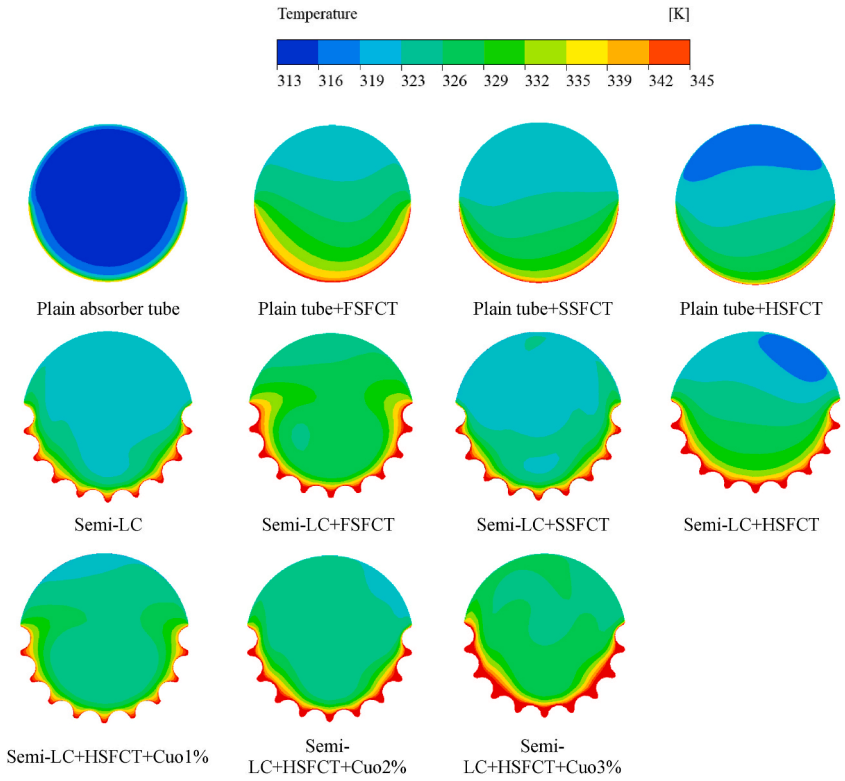

Fig. 13. Temperature contour for various cases.

plain absorber tube at a Reynolds number of 4500 can enhance the Nusselt number by up to 272 %, 186 % and 172 %, respectively. When these turbulators are incorporated into a semi-LC absorber tube with a corrugation radius of 1.5 mm (the optimal design), at the same Reynolds number of 4,500, the Nusselt numbers can be enhanced by 369 %, 275 %, and 269 %, respectively.

Regarding the frictional coefficient (see Fig. 10 (b)) when integrating FSFCT, SSFCT, and HSFCT into a plain absorber tube, the friction coefficients show increases of up to 1120 %, 420 %, and 190 %. In the case of the semi-LC tube, the increases were 1250 %, 220 %, and 502 % respectively. The impact of the shell form cone turbulator on the friction coefficient and pressure drop can be explained by three main mechanisms. First, the interaction of the fluid with the wall of the shell form cone turbulator leads to a frictional pressure drop. Second, the turbulator blocks the flow path, impeding the flow's advancement, which in turn increases the pressure drop. Furthermore, the turbulence created by the rotational and eddy currents formed behind the shell form cone turbulator intensifies the pressure drop. As shown in Fig. 15, the greatest pressure drops were recorded for the simple tube with FSFCT and the semi-LC tube with FSFCT, SSFCT, and HSFCT, respectively. It is important to note that although the effects of SSFCT and HSFCT on heat transfer are quite similar, the difference in pressure drops resulting from their presence is significant, due to the varying characteristics of the swirling and eddy currents produced by these two turbulators.

As illustrated in Fig. 11, the results show that the highest PEC is 2.51, which was specifically recorded for the semi-LC absorber tube equipped with the HSFCT. This suggests that, although the FSFCT has the most substantial impact on heat transfer, the HSFCT is the better option overall. This is because it balances both heat transfer enhancement and pressure drop, resulting in its superior PEC.

By identifying the HSFCT as the optimal geometry from a PEC standpoint, the synergistic effects of utilizing the HSFCT in conjunction with the semi-LC absorber tube and CuO-water nanofluid are also examined. The findings suggest that the combined utilization of these three approaches, while a CuO-water with a 3 % volume fraction is utilized, can boost heat transfer by up to 335 % that of a plain tube, while the friction coefficient can increase by 290 % higher than that of a simple tube. Furthermore, the PEC reaches its maximum value of 2.77 at a Reynolds number of 4300, signifying that the simultaneous application of these three techniques represents the optimal strategy. Additionally, a reduction in the nanofluid's volume fraction leads to lower Nusselt numbers and friction coefficients.

The shell form cone turbulator enhances heat transfer by partially occupying the tube's inner space, increasing fluid velocity at specific cross-sections, and directing flow towards the absorber tube wall upon impact. Its unique geometry promotes robust radial flows and increases the frequency of working fluid particle interactions with the wall, as illustrated by the streamlines in Fig. 12. Furthermore, it facilitates mixing between cooler central fluid and warmer fluid near the wall, leading to a more uniform temperature distribution across the tube cross-section. This mixing increases the temperature differential between the tube wall and the fluid, boosting heat transfer efficiency. As can be seen from Fig. 13, the average outlet temperature rises significantly, as confirmed by a comparative analysis that shows the turbulator-equipped tube (using CuO-water nanofluid) achieves notably higher outlet

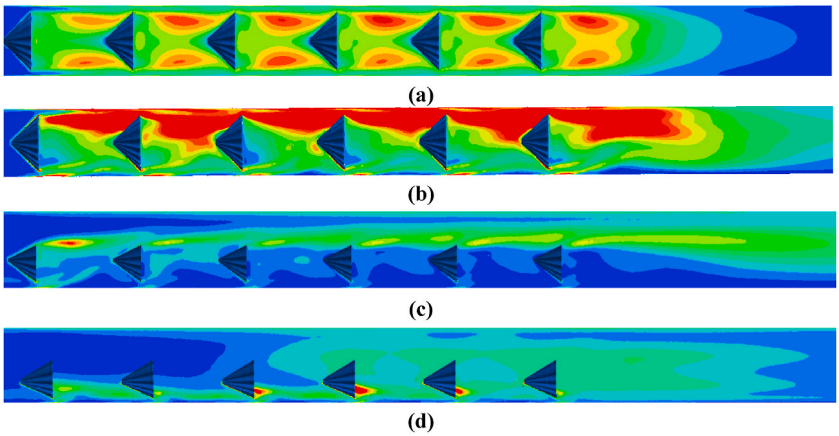

Fig. 14. Turbulence kinetic energy in the plain tube equipped with FSFCT (a) and the Semi-LC tube equipped with FSFCT (b), SSFCT (c), and the HSFCT (d).

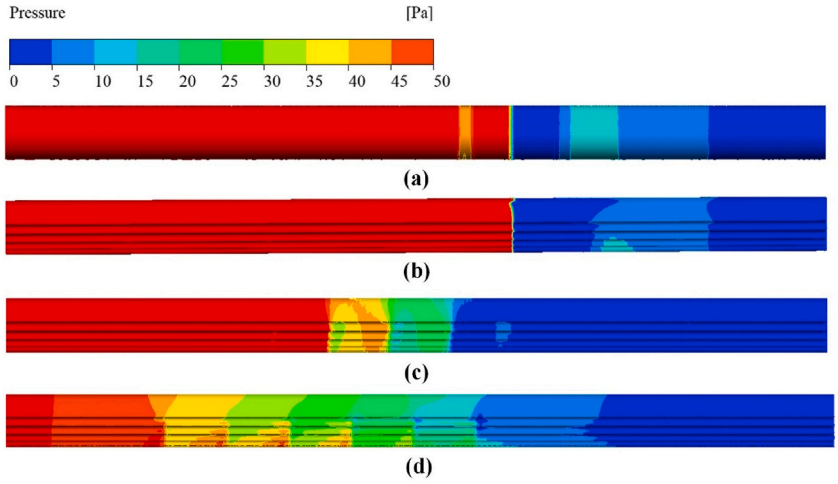

Fig. 15. Pressure contour in the plain tube equipped with FSFCT (a) and the Semi-LC tube equipped with FSFCT (b), SSFCT (c), and the HSFCT (d).

temperatures than both a plain tube and a semi-LC tube.

Results indicated that FSFCT, SSFCT, and HSFCT had the highest heat transfer rates. Notably, the streamlines illustrated in Fig. 12 indicate that SSFCT significantly impacts a substantial portion of the flow, including the middle flow and the flow around the upper and lower walls of the absorber tube. In contrast, the effects of SSFCT and HSFCT are primarily concentrated on the middle flow and the lower wall flow. Furthermore, the most pronounced swirling and eddy currents occur behind the FSFCT, followed by SSFCT and HSFCT, suggesting that heat transfer is highest in the presence of FSFCT compared to the other geometries. It is important to note that the external geometries of SSFCT and HSFCT are quite similar, yet the HSFCT's hollow structure enhances its aerodynamic profile, resulting in comparatively lower rotational and eddy currents and, ultimately, a slight reduction in heat transfer relative to SSFCT. The turbulence kinetic energy contours are illustrated in Fig. 14, further corroborating the previously obtained results. The data indicate that the highest intensity of turbulence is observed within the Semi-LC tube that is equipped with the FSFCT Combined Tube.

3.5. Economic analysis

In the final phase of this study, an economic analysis was conducted after identifying the optimal choice based on hydrothermal performance, specifically using the PEC. This analysis employed two key economic parameters, the levelized cost of energy (LCOE) and payback time, to determine the most cost-effective option. Lower values for both parameters indicate a more economical choice. Fig. 16 illustrates the LCOE and payback time for all configurations examined. In the most favorable scenario, which corresponds to the Reynolds number of 4,500, the LCOE values for the various absorber tube designs were as follows: 2.21 $/kWh for the plain absorber tube, 0.74 $/kWh for the LC absorber tube, 0.67 $/kWh for the TC absorber tube, and 0.74 $/kWh for the semi-LC absorber tube. Among the three turbulator geometries investigated, the semi-corrugated absorber tube with a 1.5 mm corrugation radius with

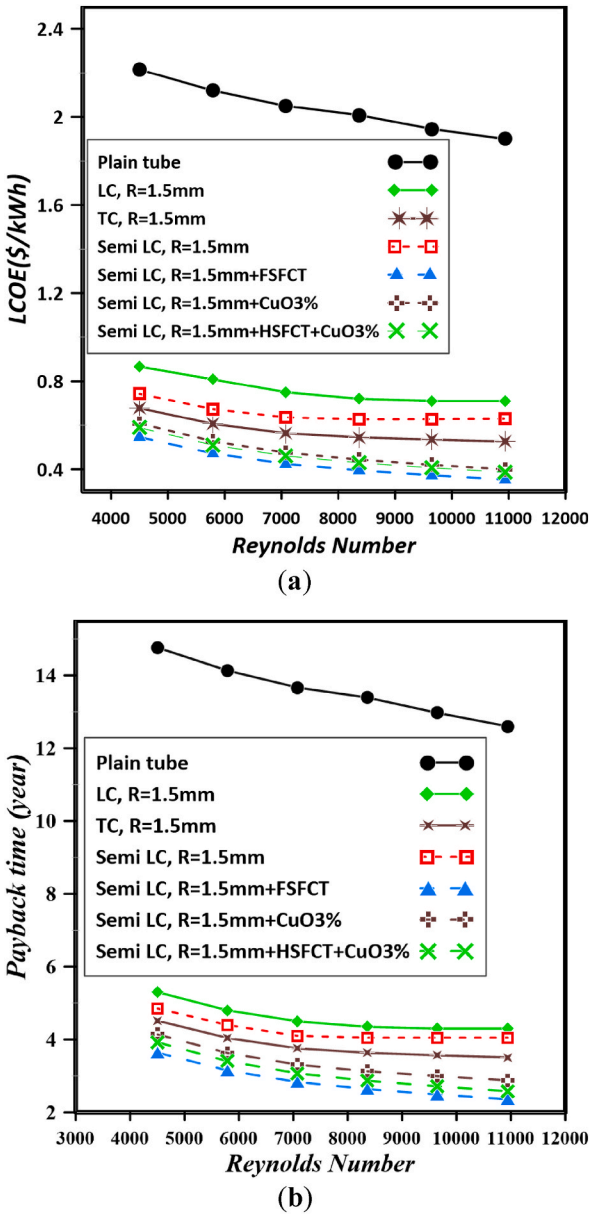

Fig. 16. Variation of the LCOE (a) and payback time (b) for various cases.

Table 1
A brief finding of the study.

Study	frictional ratio	heat transfer enhancement (%)	PEC	LCOE ($/kWh)	Pay-back time(years)
Longitudinal or transverse corrugation	LC, R = 0.5 with f/f_0 = 1.9	TC, R = 1.5 with 244 % increase	LC, R = 1.5 With PEC = 2.38	TC, R = 1.5 with LCOE = 0.764	TC, R = 1.5 with payback time = 4.5
Adding CuO nanoparticles to the base fluid	Semi-LC, R = 1.5, CuO 1 % with f/f_0 = 2.35	Semi-LC, R = 1.5, CuO 3 % with 302 % increase	Semi-LC, R = 1.5, CuO 3 % with PEC = 2.67	Semi-LC, R = 1.5, CuO 3 % with LCOE = 0.620	Semi-LC, R = 1.5, CuO 3 % with payback time = 4.14
Adding a shell form turbulator	Semi-LC, R = 1.5, HSFCT with f/f_0 = 3.2	Semi-LC, R = 1.5, FSFCT with 369.3 % increase	Semi-LC, R = 1.5, CuO 3 %, HSFCT with PEC = 2.77	Semi-LC, R = 1.5, HSFCT with LCOE = 0.545	Semi-LC, R = 1.5, FSFCT with payback time = 3.64

FSFCT's insert exhibits the lowest LCOE of 0.545 $/kWh and the shortest payback time of 3.65 years. Meanwhile, when HSFCT is combined with a 3 % CuO-water nanofluid, it achieves an LCOE of 0.608 $/kWh and exhibits the shortest payback time of 4.05 years when the inlet Reynolds number is 4500.

In conclusion, to achieve the highest Nusselt number and maximize economic performance, the optimal choice is the semi-LC absorber tube paired with the FSFCT. However, when considering optimal performance based on a balance of heat transfer and friction coefficient, the semi-LC absorber tube paired with the HSFCT + CuO 3 % configuration yielded the best hydrothermal performance, with a PEC of 2.77.

Table 1 encapsulates the overall findings of the study. It is essential to point out that this table illustrates the results for an inlet Reynolds number of 4500, providing a swift reference for industrial stakeholders to identify their preferred requirements and priorities related to thermal performance or economic considerations.

4. Conclusion

This study explores the effects of utilizing a semi-LC absorber tube on hydrothermal and economic parameters of PTSC for the first time. The findings are compared against those of standard plain absorber tubes, LC tubes, and TC tubes, offering valuable insights into performance enhancements. The analysis was conducted over a Reynolds number range of 4500 to 10,900 and for a corrugation radius from 0.5 mm to 1.5 mm. Furthermore, the synergistic effects of employing the semi-LC absorber tube in conjunction with CuO-water nanofluid at volume fractions ranging from 1 % to 3 %, along with integrating an FSFCT, SSFCT, or HSFCT within the absorber tube, were thoroughly assessed. The optimal configuration was identified from both hydrothermal and economic perspectives. Key findings are as follows.

- The TC absorber tube with a 1.5 mm corrugation radius outperformed other absorber tube geometries, boosting the Nusselt number by 244 % and the friction coefficient by 251 % compared to the plain absorber tube.
- The results indicate that increasing the corrugation radius increases Nusselt numbers and friction coefficients.
- From a PEC standpoint, the LC absorber tube, boasting a peak PEC of 2.38, clearly outperforms the TC absorber tube, which has a maximum PEC of 2.26.
- Integrating CuO nanoparticles into the working fluid significantly enhances the Nusselt number, friction coefficient, and PEC. Moreover, higher volume fractions of these nanoparticles lead to even greater improvements in these critical parameters.
- This study found that the semi-LC absorber tube with an FSFCT had a maximum Nusselt number and friction coefficient of 369 % and 1350 % higher than the plain absorber tube. It also achieved an optimal LCOE of 0.546 $/kWh and a payback period of 3.6 years, making it the most cost-effective option.
- The semi-LC absorber tube, utilizing a 3 % CuO-water nanofluid in conjunction with an HSFCT, achieves a maximum PEC of 2.77. This configuration is identified as the optimal case from a hydrothermal perspective.

CRediT authorship contribution statement

Sarminah Samad: Writing – original draft, Validation, Software. **Salman Saeidlou:** Writing – original draft, Resources, Data curation. **M. Nadeem Khan:** Writing – review & editing, Investigation. **Ali Alamry:** Writing – original draft, Data curation. **Laila M. Al-Harbi:** Writing – original draft, Resources, Formal analysis. **Mohsen Sharifpur:** Writing – review & editing, Supervision. **S.P. Ghoushchi:** Writing – original draft, Methodology.

Limitations and suggestions for future studies

A significant concern with the installation of turbulators is the heightened system pressure drop, which results in the demand for more pump power. Furthermore, such nanofluids are costly and tend to settle as time passes. This research can be integrated with recent studies, such as those utilizing advanced nanofluids like carbon-walled nanotubes, which exhibit significantly reduced sedimentation. Additionally, it may involve employing different turbulators that are compatible with this type of tube or modifying the tube's geometry to a flat design with corrugation.

Declaration of competing interest

With the submission of this manuscript, I would like to undertake that the manuscript has not been published elsewhere, accepted for publication elsewhere or under editorial review for publication elsewhere.

Acknowledgment

The research is supported by Princess Nourah bint Abdulrahman University Researchers Supporting Project number (PNURSP2025R4), Princess Nourah bint Abdulrahman University, Riyadh, Saudi Arabia.

Data availability

Data will be made available on request.

References

[1] S. Alshehery, Q. Al Mdallal, A.A. Altohamy, L.B. Said, M. Bouzidi, T. Alkathiri, L. Kolsi, Case Stud. Therm. Eng. (2025) 105849.
[2] Z. Zhao, F. Bai, X. Zhang, Z. Wang, Sol. Energy 207 (2020) 91–102.
[3] M.S. Nazir, A. Shahsavar, M. Afrand, M. Arıcı, S. Nižetić, Z. Ma, H.F. Öztop, Sustain. Energy Technol. Assessments 45 (2021) 101103.
[4] M. Arun, D. Barik, H. Ahmad, I. Alraddadi, M.A. Shenashen, Z.A. Khan, Case Stud. Therm. Eng. 61 (2024) 104840.
[5] A. Alhamayani, Case Stud. Therm. Eng. 57 (2024) 104321.
[6] A. Alhamayani, M. Al-lehaibi, Case Stud. Therm. Eng. 59 (2024) 104593.
[7] R. Elarem, T. Alqahtani, S. Mellouli, W. Aich, N.B. Khedher, L. Kolsi, A. Jemni, Case Stud. Therm. Eng. 24 (2021) 100859.
[8] B. Kumar, A. Awasthi, J. Lee, Y. Jeon, Case Stud. Therm. Eng. 66 (2025) 105783.
[9] W. Fuqiang, T. Zhexiang, G. Xiangtao, T. Jianyu, H. Huaizhi, L. Bingxi, Energy 114 (2016) 275–292.
[10] A.A. Al-Rashed, A.A. Alnaqi, J. Alsarraf, J. Taiwan Inst. Chem. Eng. 124 (2021) 192–204.
[11] M. Zaboli, S.S. Mousavi Ajarostaghi, S. Saedodin, M. Saffari Pour, Appl. Sci. 11 (2021) 7423.
[12] T. Limboonruang, M. Oyinlola, D. Harmanto, N. Phunapai, Appl. Therm. Eng. 263 (2025) 125317.
[13] S. Samad, S. Saeidlou, I. Mahariq, N. Kraiem, A. Alamry, P.A. Hoskeri, S. Ghoushchi, Case Stud. Therm. Eng. (2025) 106462.
[14] B. Stanek, J. Ochmann, D. Węcel, Ł. Bartela, Energies 16 (2023) 3716.
[15] Y. Jebbar, F. Fluiful, W. Khudhayer, Fluid Dynamics & Materials Processing, vol. 20, 2024.
[16] R. Venkatesaperumal, K. Syed Jafar, P.V. Elumalai, M. Abbas, E. Cuce, S. Shaik, C.A. Saleel, Sustainability 15 (2022) 378.
[17] A. Painuly, G. Joshi, P. Negi, P. Zainith, N.K. Mishra, Int. J. Therm. Sci. 208 (2025) 109399.
[18] A. Painuly, N.K. Mishra, P. Zainith, R. Das, Numer. Heat Transf. A Appl. 86 (2025) 687–708.
[19] A. Painuly, N.K. Mishra, P. Zainith, J. Therm. Anal. Calorim. 149 (2024) 3965–3980.
[20] P.K. Namburu, D.P. Kulkarni, D. Misra, D.K. Das, Exp. Therm. Fluid Sci. 32 (2007) 397–402.
[21] M.H. Mosavian, S.Z. Heris, S.G. Etemad, M.N. Esfahany, J. Nanoparticle Res. 12 (2010) 2611–2619.
[22] A.Y. Bhat, A. Qayoum, Thermochim. Acta 714 (2022) 179267.
[23] S. Alshehery, Q. Al Mdallal, A.A. Altohamy, L. Ben Said, M. Bouzidi, T. Alkathiri, L. Kolsi, Case Stud. Therm. Eng. 67 (2025) 105849.
[24] S. Samad, S. Saeidlou, I. Mahariq, N. Kraiem, A. Alamry, P.A. Hoskeri, S.P. Ghoushchi, Case Stud. Therm. Eng. (2025) 106462, https://doi.org/10.1016/j.csite.2025.106462.
[25] M. Jafaryar, M. Sheikholeslami, Renew. Energy 198 (2022) 534–548.
[26] M. Aliehyaei, A.H. Joshaghani, M.M. Najafizadeh, Eng. Anal. Bound. Elem. 150 (2023) 492–506.
[27] N. Mashoofi, S. Pourahmad, S.M. Pesteei, Case Stud. Therm. Eng. 10 (2017) 161–168.
[28] M.E. Nakhchi, J.A. Esfahani, J. Therm. Anal. Calorim. 145 (2021) 2535–2545.
[29] F. Vahidinia, A. Aghaei, H. Khorasanizadeh, J. Heat Mass Transf. Res. 12 (2025) 209–226.
[30] W. Al-Aloosi, Y. Alaiwi, H. Hamzah, Case Stud. Therm. Eng. 49 (2023) 103378.
[31] P. Liu, N. Zheng, Z. Liu, W. Liu, Energy Convers. Manag. 179 (2019) 30–45.
[32] M.Y. Al Shdaifat, R. Zulkifli, K. Sopian, A.A. Salih, Micromachines 11 (2020) 416.
[33] N.M. Maleki, S. Pourahmad, E. Tavousi, N. Perera, P. Talebizadehsardari, A. Keshmiri, Int. Commun. Heat Mass Tran. 161 (2025) 108406.
[34] M. Malekan, A. Khosravi, S. Syri, Appl. Therm. Eng. 163 (2019) 114435.
[35] A. Hosseini Esfahani, M. Aliehyaei, A. Hassani Joshaghani, M.M. Najafizadeh, Energy Eng. Manage. 12 (2023) 80–99.
[36] A. Kasaiean, M. Sameti, R. Daneshazarian, Z. Noori, A. Adamian, T. Ming, Renew. Energy 123 (2018) 439–449.
[37] R. Suresh Isravel, M. Raja, S. Saravanan, V. Vijayan, Mater. Today Proc. 21 (2020) 127–129.
[38] A. Lintermann, in: Clinical and Biomedical Engineering in the Human Nose: A Computational Fluid Dynamics Approach, Springer, 2020, pp. 85–115.